> ID 2024-EMC-0163 <

Broken Rotor Bar Detection in Closed Loop Inverter Fed Induction Motors Through Time-Frequency Techniques

Lorenzo Mantione, *Student Member*, *IEEE*, Tomas Garcia-Calva, *Member, IEEE*, Vanesa Fernandez-Cavero, Lucia Frosini, *Member, IEEE,* and Daniel Moriñigo-Sotelo, *Member, IEEE*

***Abstract*— In traction, automotive, and some industrial processes, the operation of the induction motor is set using speed. This creates an additional control loop that is external to the current controller that inverters already possess. While the impact of the latter control loop on fault detection in induction motors has already been studied, the influence of closed-loop speed control has not been explored enough. This paper presents the findings on the impact of PID speed control on the broken rotor bar fault detection. The study reveals that the constant corrective actions of the PID controller to correct the speed cause an increase in the noise level and spectral leakage around the first harmonic in the stator current spectrum that prevents fault detection. It is concluded that it is necessary to use time-frequency analysis techniques with excellent spectral resolution, such as the Dragon Transform or the Min-Norm technique.**

***Index Terms*— Induction motor, inverter, speed closed-loop control, fault detection, time-frequency analysis.**

I. INTRODUCTION

Induction motors are the primary means of obtaining mechanical energy in industry. They are also used in other areas such as railway transport, automotive, and service sectors (elevators, pumping systems, and air conditioning systems). As is well known, their use is based on their robustness and low cost. However, they can also suffer from failures resulting in production or service downtime and associated economic costs, including replacement and repair costs. Elements or components that can fail include bearings, stator insulation, shaft, and rotor cage (bars and end rings).

The Electrical Engineering Department of the University of Valladolid (UVa), the Research Group ADIRE, and the ITAP Institute have partially funded this work. The author Lorenzo Mantione was benefited from an Erasmus+Traineeship grant that allowed him to stay at UVa.

L. Mantione and Lucia Frosini are with Department of Electrical, Computer and Biomedical Engineering, University of Pavia, 27100 Pavia, Italy. (e-mail: lorenzo.mantione01@universitadipavia.it, lucia.frosini@unipv.it).

T. Garcia-Calva is with Research Group HSPDigital and the Department of Electrical Engineering, University of Valladolid, Valladolid, VLL 47001 ES (e-mail: tomasalberto.garcia@uva.es).

V. Fernandez-Cavero is with the Department of Electromechanics Engineering, University of Burgos, Burgos, 09001 ES (e-mail: vfcavero@ubu.es).

D. Morinigo-Sotelo is with Research Group HSPDigital-ADIRE, ITAP, University of Valladolid, Valladolid, VLL 47001 ES (e-mail: daniel.morinigo@eii.uva.es).

Color versions of one or more of the figures in this article are available online at http://ieeexplore.ieee.org

Broken rotor bars (BRB) and cracked end rings are responsible for 5-10% of squirrel cage induction motor failures. Despite their low occurrence rate, detecting these faults is crucial as they can cause serious secondary effects. Broken fragments may impact the stator winding, causing severe damage to its insulation. In addition, the redistribution of the currents in the adjacent bars increases thermal stress, leading to a slowly progressive fault propagation. Therefore, diagnostics can help prevent such issues. As a result, extensive research has focused on developing methods for detecting this fault [1],[2]. The manufacturing process of the rotor affects the likelihood of its failure. Depending on the assembly method, rotor can be die-cast or fabricated. The former is considered more robust and less prone to break. In the latter, the point of connection between the bars and the end ring is the weakest point, making it more susceptible to failure. There is a third and more specific case, which is deep well submersible pumps. Their rotor is made with manufactured copper bars, but the short-circuit ring is different and not solid. It is formed by several laminated and stacked copper sheets. Rotor high-speed and internal cooling water frequently make this end ring fall apart [3].

Though most research on this fault has focused on motors powered by the mains [4], it is now important to consider motors that are fed by electronic converters, particularly in closed-loop operation. Speed can be used as a reference signal to set the motor power supply in some industrial and traction applications, including automotive. This creates an additional external control loop beyond the current control that inverters already possess and whose impact on the detection of broken rotor bars has already been studied. In closed-loop operation, the current controller guarantees a safe operation even when both stator and rotor windings are imbalanced. Thus, the compensating action of this control system decreases the typical fault harmonics in the stator current [5]. Two studies on the topic were published in 2000 [6], [7]. Research in [6] shows that the frequency spectrum of the i_d field current component in a Field-Oriented Controlled (FOC) induction motor is a useful diagnostic index. Simulation and experimental results show that the amplitudes of the spectrum components at frequencies $2f_s$ and $2sf_s$, where f_s is the main supply frequency and s is the slip, are almost constant with proportional gain variations. They are also quite linearly dependent on stator and rotor fault severities. Therefore, these fault indicators are quite independent of the control parameters for the topology of the control system adopted, i.e., Direct

Rotor Field-Oriented Control (DRFOC), and for a fixed bandwidth of the flux control loop.

Researchers in [7] proposed a diagnostic technique, named Vienna Monitoring Method (VMM), to detect BRB in a vector-controlled induction motor by computing two electromagnetic torque-related values using a model based on voltages and currents. In [8], the VMM was further improved, making it possible to implement it without a position sensor. However, certain aspects related to the applicability of this method still require investigation, such as the effect of tuning the current, flux, and speed controllers of the drive. In [9], the behaviour of the magnetising current component i_d was analysed for three types of vector-controlled drives. The study found that this quantity can be utilised to detect BRB in Indirect Rotor Field-Oriented Control with a Flux Control loop (IRFOC-FC) and DRFOC drives. However, the amplitude of the fault indicator is not the same for these two types of control systems, and it is dependent on the parameters of the flux controller. Reference [10] proposed a model-based technique to detect and quantify the BRB fault. This technique is effective and independent of the operating conditions, such as load level, reference speed, and bandwidth of the control loops. However, it is only valid for specific current control strategies. A completely different approach is reported in [11], where the detectability of BRB in Indirect Rotor Flux Oriented Control (IRFOC) is studied for variable speed double cage induction motors, using vibration signature analysis techniques. This paper examines the control system's impact on the fault harmonics relevance in the axial and radial vibration signals. Axial vibration analysis shows a more robust fault signature under the control action in distinguishing the healthy rotor condition from BRB in double squirrel cage induction motors. In [12], the stator line current is analysed by means of a combination of empirical mode decomposition (EMD) and Wigner-Ville distribution (WVD) to detect BRB fault in open and speed closed-loop control, along with a two-hidden layer feed-forward artificial neural network. This technique is preliminarily tested through finite element simulations and then experimentally with a simple closed-loop system. It proved to be successful only when the motor was under full load and had two broken bars. In [13], a new online diagnosis method, based on both currents and voltages, is proposed to detect BRB in a closed-loop controlled induction motor. Since the stator current fault harmonics propagate to voltage in a closed-loop, a fault severity factor is proposed to evaluate the extension of the fault obtained from the left sideband components and the fundamental ones of the motor currents and voltages. In [14], the same research group proposed a method to detect and quantify BRB using zero-sequence voltage in a wye-connected induction motor in both open- and closed-loop.

In [15], the diagnosis of a 22 kW induction motor operating in closed-loop, under State Vector Control (SVC) based Direct Torque Control (DTC) mode, with one, two and three broken bars, was presented. Instead of the classical Fast Fourier Transform (FFT), the authors propose the FFT analysis of the current envelope, the Park's vector plot of the current and the FFT analysis of the Park's vector modulus. They determine that Park's vector method provides more insightful diagnostic information despite the significant presence of inverter-fed harmonics in the Park's vector modulus. Also, in [16], it was found that the conventional Motor Current Signature Analysis (MCSA) is not able to detect BRB when the induction motor is supplied by an inverter at low load conditions because the fundamental harmonic of the current hides the harmonic sidebands induced by the fault. For this reason, the authors experimentally investigated other methods, like Hilbert Transform, Synchronous Demodulator, Teager Kaiser Energy Operator, and Peaks Detection Envelope, but without indicating whether the motor was operating in an open- or closed-loop. Even in [17], the authors simply refer to an inverter-fed induction motor and state that switching harmonics compromise the reliability of MCSA in detecting BRB. Therefore, they propose the standstill impedance variation test to verify whether the BRB fault introduces some form of asymmetry. On the contrary, in [18], the authors evaluate a new technique to detect BRB in both open- and closed-loop. This approach is called AWSTE and combines estimating signal parameters via rotational invariance techniques (Esprit) and the adaptive window strategy to estimate the instantaneous fundamental frequency. In addition to the literature analysed above, suggestions on suitable techniques for use in closed loop may come from research on the diagnostics of Permanent Magnet Synchronous Machines (PMSMs), which always operate in closed loop. Some interesting recent works are [19]-[21], but the faults considered are obviously different, and therefore, the proposed approach should be carefully evaluated before being applied to induction machines.

Based on the literature review presented above, the aim of this work, which extends a previously published study [22], is to develop a method to detect BRB in induction motors operating under closed-loop speed control. The method should overcome the difficulties imposed by the time-varying corrective action of controllers, rely mainly on measurements available in inverters, suitable for different control settings and generalizable as possible. Although die-cast rotors infrequently exhibit breakage of the bars, they can be used in the laboratory to validate diagnostic procedures for fabricated rotors. In this research, the die-cast rotor of an induction motor has been modified by drilling a hole in its end ring to simulate a bar breakage and avoid magnetic imbalances in the lamination. Experimental analysis of the current signal will reveal that spectral analysis with the FFT that seeks to detect frequency bands around the first harmonic cannot distinguish the fault when the motor is powered by an electronic converter operating with a cascade-structured control. This is tested for the first time using two different PID controllers (underdamped and overdamped). Since traditional MCSA with FFT fails, it is abandoned in favour of time-frequency approaches like Short Time Fourier Transform (STFT) [23], Dragon Transform [24] and Min-Norm algorithm [25].

II. Theoretical Background

A. Closed-loop System

Inverter-fed induction motors can run in closed-loop. The control signal can be the speed or a process signal. When operating in closed-loop, there are actually two control loops (see block diagram in Fig. 1) [26]. The first is an internal control loop of the inverter that is used to set the motor's feed current. It is a very fast control loop (total delay estimates are between 1.5 to 2 times the sampling period [13], [26]) and can implement the techniques mentioned in the Introduction. This

control loop also acts on motors operating in open-loop (no speed control signal or process signal), and the most commonly used techniques in both cases are scalar control, FOC, or DTC. The latter two require the speed signal, although there are sensorless variants [27]. When a speed or process signal control is fixed, a second control loop is established, which is external and slower than the previous one [13],[26]. This type of control with two loops is known as a cascaded control structure. Its purpose is to keep the controlled signal at a fixed value, regardless of motor load changes, which are treated as disturbances. PI and PID are the most common controllers, for which many tuning procedures have been developed that require knowing the plant's transfer function. When this is unknown (as is this case), methods such as the Ziegler-Nichols method can be adopted, which involves the plant being brought to its stability limit. In the case under study, this was not possible, and the Internal Model Control (IMC) method was used [28]. In this technique, the open-loop plant is subjected to a step input, which is a start-up in the case of an electric motor [29]. The IMC allows a choice of controller type. The PID can be tuned to provide a fast or underdamped response or a slower or overdamped response, depending on the dynamic requirements of the drive.

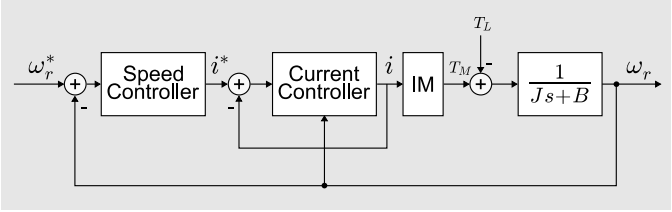

Fig. 1. Block diagram of a closed-loop control of an inverter-fed induction motor where ω_r^* = speed reference, ω_r = estimated speed signal, i^* = reference current, i = estimated current, T_M = developed torque, T_L = load torque, J = drive's moment of inertia, B = damping coefficient.

B. Analysis of non-stationary signals

B.1. Dragon Transform

This study focuses on BRB detection tracking the harmonics generated in the stator current which follow unique trajectories in the time-frequency plane. These trajectories are very close to the one described by the first harmonic generated by the power supply and, because of its high energy, it is not possible to visualize them using techniques such as the STFT [24]. Therefore, it is necessary to use more advanced techniques for their correct visualisation. For this purpose, the Dragon Transform (DT) [24] has been used in this study because it accurately tracks the trajectory of the harmonics, even when they are in close proximity to the first high-energy harmonic. It is based on time-frequency atoms, specifically on dragon atoms that are defined so that their shape is perfectly adapted to the harmonic trajectory to be followed, as specified in [24],[30]. This provides excellent time and frequency resolutions in the trajectory of interest, allowing the correct visualization of these components as very thin lines in the time-frequency plane without interference from the energy of the first component. Therefore, the DT is the correlation between the signal to be analysed with a family of dragon atoms $\phi(t)$, which are defined as follows [24]:

$$\phi(t) = \frac{1}{\sqrt[4]{\pi}\sqrt{\sigma}} e^{-\frac{(t-t_c)^2}{2\sigma^2}} e^{2\pi i\theta(t)} \quad (1)$$

where σ is a deviation parameter, t_c is the time instant where the atom is centred, and $\theta(t)$ is part of a complex exponential that defines the atom's shape. The time derivative of $\theta(t)$ follows the trajectory in the time-frequency plane of the harmonic component of interest (in this study related to the BRB fault):

$$\frac{d\theta(t)}{dt} = g\big(s(t), f_s(t)\big) \quad (2)$$

where $s(t)$ is the motor slip and $f_s(t)$ is the main harmonic, and g is a function that provides the trajectories of the fault-related harmonics. Hence, the atom is defined according to the theoretical trajectory of the fault-related component, and therefore, it needs information about the rotor speed, which is one of its drawbacks. The time-frequency decomposition $\langle h, \phi \rangle$ is computed as the correlation of the signal of interest $h(t)$ with the family of atoms:

$$\langle h, \phi \rangle = \int_{-\infty}^{+\infty} h(t)\phi^*(t)dt \quad (3)$$

B.2 Short Time Minimum-Norm

The Short-Time Minimum-Norm (STMN) algorithm is a spectral estimator based on sub-space decomposition (signal and noise spaces) that can be used to determine the harmonic content of time-domain signals. The estimator considers M points of a continuous-time signal $s(t)$, which is sampled with a constant time period. At a certain time instant t, the signal can be modelled as:

$$s(t) = \sum_{p=1}^{P} \varphi(\omega_p) s_p(t) + \eta(t) \quad (4)$$

where $s_p(t)$ denotes the p-th harmonic component in the signal's spectrum, φ is a uniformly sampled complex sinusoid array, and $\eta(t)$ is the measurement noise. Based on orthogonality of signal spaces, the estimator can analyse time-varying multi-component series. The time-frequency decomposition of $s(t)$ is given by:

$$Sxx(t, \omega) = \sum_{n=0}^{m=Nd-1} \frac{s(t)w(t - \tau l)}{\sum_{p=1}^{P} |\varphi(\omega)\omega^2|} \quad (5)$$

where N_d is the data length of a sliding window analysis, w, of the time signal $s(t)$, l is the leap size between successive windows, p is the number of frequency components inside the signal, and ω is the frequency index [25],[31]. STMN analysis provides good performance and, in general, requires more computational time than classic spectral estimators (such as

Fourier transform-based) but less than non-linear or adaptive transformations (Wigner-Ville or DT). Unlike DT, STMN does not require information on the rate of change of frequency of the components within the signal to analyse. This makes STMN a useful high-resolution technique for the time-frequency decomposition of time-varying current signals.

III. Test Bench

The experimental setup (Fig. 2.a) consists in two star-connected 4 poles 2.2 kW squirrel cage induction motors from ABB (3GAA102213-ASE; rated speed 1450 rpm; rated torque 14.40 Nm) fed by a Danfoss (VLT Midi Drive FC 280) voltage source inverter (VSI) in speed closed-loop operation. In each test, one of the two motors is coupled through an elastic joint to a Delco Remy DC alternator used as a mechanical load. The load torque is modified by inserting and removing banks of resistors in the stator circuit of the alternator. The rated line voltage of the motor is 400 V. To simulate the fault, the rotor of one induction motor has been modified by drilling a hole in the squirrel cage end ring at a rotor bar end to avoid rotor lamination damage, that can lead to undesired magnetic unbalances in the motor during operation (Fig. 2.b). This operation allowed to increase the resistance of the bar simulating a breakage. The stator phase current is acquired by a Hall effect transducer connected to a NI data acquisition system (DAS). Closed-loop control is allowed using an Omron 500 PPR incremental encoder (model E6C2-CWZ1X), which is a significant difference compared to a later work [32] in which a 1024 PPR encoder was used. The encoder signal is sent to the inverter and includes white noise from the feedback loop [33].

The speed control consists in a PID controller implemented in the inverter and tuned to ensure fast response to a system variation. The PID transfer function is:

$$R_{PID}(s) = K_P\left[1 + \frac{1}{sT_i} + sT_d\right] \quad (6)$$

where K_P is the proportional gain, T_i is the integral time and T_d is the differentiation time of the speed controller.

Two different PID controllers tuned using the IMC experimental method have been tested [28], [29]. One controller provides an underdamped, more unstable response and reacts quickly to system disturbances: it is called "fast controller". The second one provides an overdamped response, more stable and slower than the previous one, and is called "slow controller". Their configuration parameters are shown in Table I, and Fig. 2.c shows their different responses to a speed step input, which is the start-up of the motor. The speed response of the motor will undergo constant variations due to the PI action of the controller [34], [35]. The magnitude of these speed disturbances will depend on the inertia of the drive, which in this case is low (0.009 kg/m^3) [36]. These speed variations and main frequency corrections from the controller affect the slip, which would not be constant and, therefore, will also affect the observation of fault harmonics in the current spectrum. The study of two PID controllers permitted to assess how these variations in speed due to the controllers' actions will affect the detection of BRB fault harmonics.

Laboratory tests were carried out by collecting 20 s long signals with a sampling frequency of 100 kS/s, including the start-up transient, in order to have the same condition in the control loop for all the analysed cases (the start-up transient was not considered in this study), and only the last 10 s of the signals were analysed. Before the spectral analysis, signals were resampled to reduce the analysis frequency range and decrease the computational time for both the Fast Fourier analysis and time-frequency transformations. Tests were carried out at different frequencies (30 to 60 Hz), but only those at 50 Hz are shown in this study.

TABLE I
PARAMETERS OF THE PID CONTROLLERS

	K_P	T_i [s]	T_d [s]
Fast Controller (FC)	0.300	0.033	0.0165
Slow Controller (SC)	0.692	0.3925	0.0945

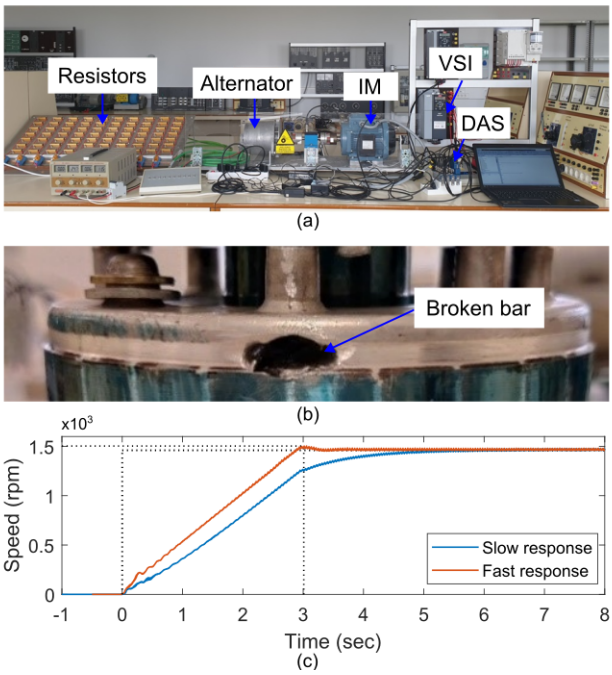

Fig. 2. Laboratory test bench. (a) Test rig, (b) Drilled hole in the end ring to simulate the broken rotor bar fault, and (c) step response for fast and slow controllers.

IV. Classical Analysis with FFT and STFT

BRB can be detected by identifying the following harmonic components in the stator current spectrum [25]:

$$f_{BRB} = (1 \pm 2ks)f_s \quad (7)$$

where s is the slip and k assumes integer values. When k = 1, two harmonic components around the fundamental result, which have the highest amplitude of those related to the fault and are known as lower sideband harmonic (LSH, $(1-2s)f_s$) and upper sideband harmonic (USH, $(1+2s)f_s$).

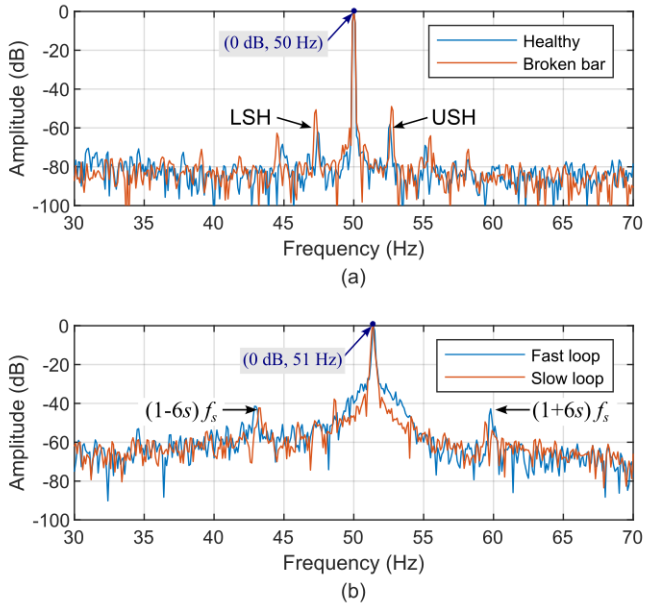

Fig. 3. Spectra of motors at steady state: (a) Open-loop control for healthy (blue) and faulty case (orange); (b) Fast (blue) and slow (orange) closed-loop control for the faulty case.

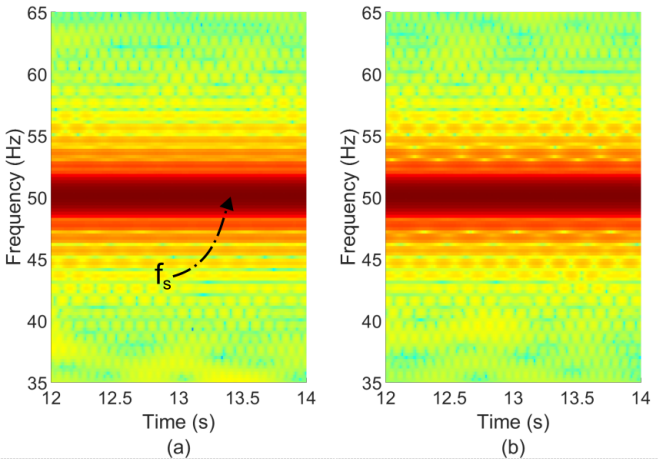

Fig. 4. STFT of motor phase-currents operating in open loop at steady state: (a) healthy motor, and (b) faulty motor.

Fig. 3.a shows stator current spectra for a healthy and a faulty motor, both operating in open loop and stationary conditions (speed = 1465 rpm and load torque = 11.3 Nm). The LSH and USH harmonics are visible, and no spectral leakage effect is observed around the fundamental, meaning that the supply frequency is fixed. The amplitude difference between the healthy and faulty cases is around 10 dB (the healthy rotor already presents a certain asymmetry level). Finally, the noise level of the signal is low, around -80 dB. Fig. 3.b shows the current spectra of the faulty motor operating in a closed loop under the action of the two controllers and the same load level as results of Fig. 3.a. The output frequency setpoint is 50 Hz, and to compensate for the speed drop due to the load torque, the controllers increase the fundamental frequency to 51 Hz. As predicted by the noise in the sensed speed, a higher noise level is observed (floor is around -65 dB), which could make it difficult to observe low-amplitude harmonics. A similar effect to spectral leakage is also observed around the fundamental harmonic. This is due to the constant action of the controller introducing fast variations of the fundamental frequency. As expected, this effect is more pronounced for the fast controller and prevents the observation of fault-related harmonics. However, the third band (k = 3, Eq. 7) is observed for both controllers and LSH only with slow controller. The third band amplitude is lower than LSH and USH amplitudes but allows observing the fault in closed-loop operation because it is further away from the fundamental frequency and the frequency range suffering from the spectral leakage.

Therefore, steady-state current analysis using the FFT is insufficient to detect the fault, so it is necessary to use a time-frequency analysis technique, and the STFT, which is the simplest one, could be used [23]. STFT has a time and frequency resolution trade-off. If the frequency resolution is better, the time resolution gets worse, and vice versa. Its use is illustrated in Fig. 4, where two spectrograms with the best possible frequency resolution are shown. The detection of a fault in the time-frequency plane is based on the observation of the trajectories of the fault-related harmonics, given in this case by Eq. 7. In the case of a broken bar fault, these trajectories are very close to the one of the first harmonic, which also has the highest amplitude. Therefore, a high-frequency resolution is required to see these fault-related paths with lower energy and parallel to the first harmonic trajectory. As shown in Fig. 4, the energy of the fundamental harmonic spreads over a wide frequency range and buries the fault-related trajectories in Fig. 4.b, which corresponds to an open-loop control and the faulty motor. Therefore, in the next sections, two more modern techniques are tested to detect the fault: DT and STMN. The first allows the fault trajectory to be observed and quantified because it has excellent time and frequency resolutions, but only around the frequency component under study (Eq. 7) and needs to know the speed signal to correctly define the time-frequency atoms on which it is based. Eq. 2, which defines the shape of the atoms, is as follows for the detection of the broken rotor bars:

$$\frac{d\theta(t)}{dt} = |1 + 2ks(t)|f_s(t) \tag{8}$$

STMN is a spectral estimation technique that also has excellent time and frequency resolutions and does not require knowledge of the speed signal, although a good estimation allows for better identification of the fault harmonic trajectories.

V. Time-Frequency Analysis

A. Analysis of the Open Loop Control Case

Figs. 5 and 6 show the time-frequency (t-f) decomposition of the phase current for healthy and faulty motor, using DT and STMN techniques, respectively. The motor operated at a load torque of 13 Nm and under open-loop control. These figures show the advantages and disadvantages of each

analysis technique. As the motor runs at a constant speed, the dragon time-frequency atoms allow for observing fault-related trajectories in Fig. 5.b as very thin lines due to the excellent time and frequency resolutions. STMN also displays a good frequency resolution and enables the distinction of the trajectories in the time-frequency plane of the LSH and USH harmonics (Fig 6.b). By properly tuning these analysis tool parameters, these sidebands are absent because of their low amplitude in the time-frequency decomposition for the healthy case (Fig. 6.a). Additionally, it is important to note that the noise level in both figures is very low. The effect of the BRB on the stator current can be exploited to identify this fault by evaluating the LSH magnitude. Between the healthy and the faulty case large increments are present in the t-f analyses, i.e. 35 dB for the STMN and 25 dB for the DT.

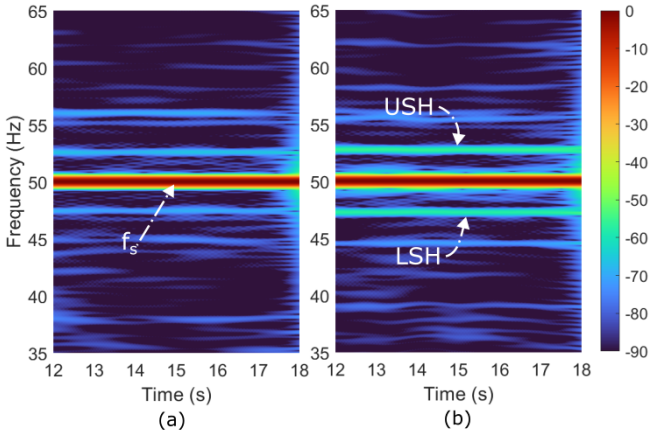

Fig. 5. Time-frequency decomposition of current using the DT in open-loop at a steady state: (a) healthy, (b) faulty.

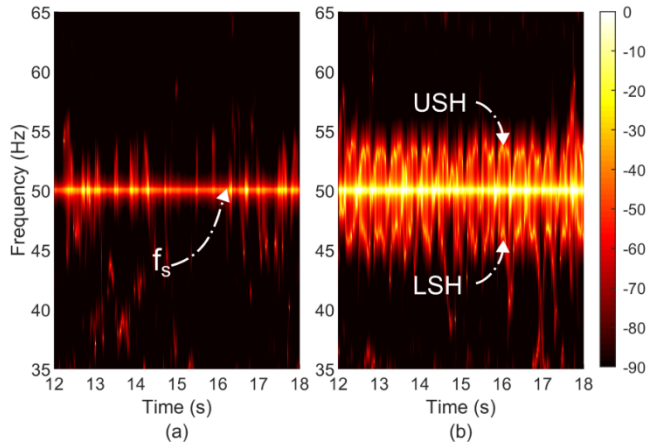

Fig. 6. Time-frequency decomposition of the current using the STMN in open-loop at steady state: (a) healthy, (b) faulty.

B. Analysis of the Closed Loop Fast Controller Case

Figs. 7 and 8 show the t-f decompositions for the case of the motor operating under the fast controller and with a constant load torque of 12.7 Nm. Fig. 7 clearly shows the advantages and disadvantages of using the DT technique. Due to the corrective response of the PI action of the controller, the fundamental frequency is not constant and changes are observed over time. Furthermore, the setpoint value is no longer 50 Hz, as the control increases it to compensate for the load torque action. However, due to its excellent resolution in both axes, the DT manages to perfectly detect the main harmonic and third band fault harmonics trajectories around 43 and 60 Hz (Fig. 7.b). However, when defining the shape of the atoms in relation to Eq. 5, as the frequency and slip (calculated from the sensed speed) undergo abrupt changes, this results in a worse definition of the rest of the frequency components. Furthermore, compared to Fig. 6, although the noise level is higher, the fault-related harmonics are observed, but not the LSH and USH.

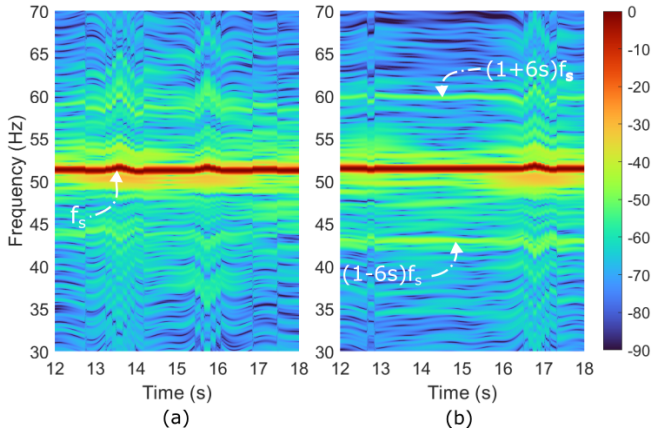

Fig. 7. Time-Frequency decomposition of the stator current using the DT with the motor operating at constant load torque and under the fast controller: (a) healthy, (b) faulty.

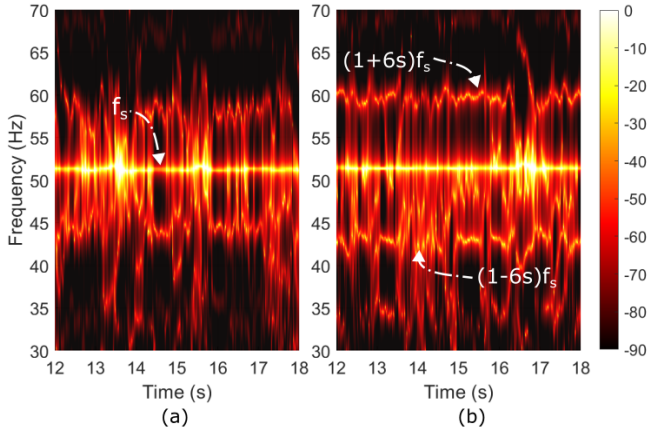

Fig. 8. T-f decomposition of the stator current using the STMN with the motor operating at constant load torque and under the fast controller: (a) healthy, (b) faulty.

Fig. 8 displays the t-f decomposition using the STMN technique for the same signals as Fig. 7. This technique's resolution allows for easy observation of the main harmonic and the third band of the fault harmonics (Fig. 8.b). Unlike the DT technique, STMN is less sensitive to noise and the components associated with the previously mentioned inherent rotor asymmetry in the healthy case are observable (they were not visible in Fig. 7.a because of the noise and shape of the atoms). In the faulty case, the energy of the sidebands is greater, leading to a better definition in the t-f decomposition.

Furthermore, the faulty motor current signal has less uncertainty and noise than the healthy case and the DT t-f decomposition. In these results (Figs. 7 and 8), t-f decompositions allowed to identify the fault harmonics, these with an amplitude increase in the magnitude of more than 20 dB between the healthy case and the faulty case. Because of the inherent asymmetries of the motor the side harmonics are expected to be present in the healthy case but with a low magnitude.

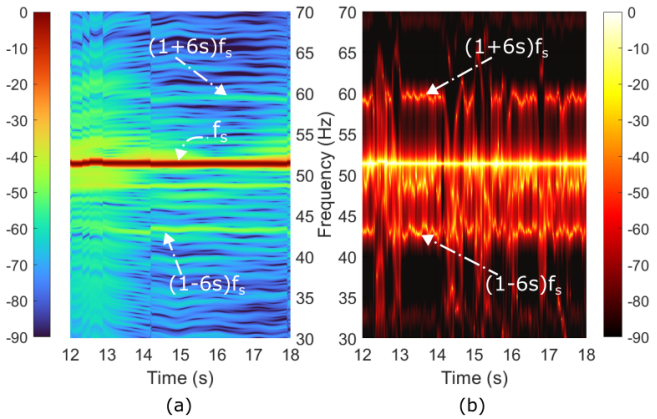

Fig. 9. T-f decompositions of the current for the faulty motor at constant torque with slow controller: (a) DT, (b) STMN.

C. Analysis of the Closed-loop Slow Controller Case

Fig. 9 shows the t-f decompositions for the case of the broken bar motor running under the slow controller with a load torque of 12.8 Nm. The D-action of the controller causes it to run overdamped, and this limits the frequency variations observed for the fast controller. Motor operation is arguably more stable, although the noise level remains high. This more stable operation allows for a better definition of the dragon atoms, which results in a cleaner t-f decomposition that allows for a precise identification of the third band and the LSH components (Fig. 9.a). This is also the case with the STMN technique (Fig. 9.b). From the t-f analyses, a strong amplitude (1-6*s*)*f*$_s$ component can be evaluated: in both distributions the fault harmonic is over -40 dB, a clear indicator of a rotor fault in the field.

D. Analysis of the Closed Loop Control with Torque Disturbance

A sudden load increase of 12 Nm was applied to the mechanical system driven by the damaged motor to assess the impact of torque disturbances on the stator current. These tests were conducted using the two PID controllers and allowed to evaluate their different responses to the disturbance. In both tests, the setpoint speed was set at 1450 rpm. The dynamic response of the speed to the applied disturbance is shown in Figs 10.a and 11.a for the fast and slow controllers, respectively. The solid cyan line corresponds to the designated speed reference, and the green line represents the generated torque disturbance. These results show that the controllers adjust and limit accurately the deviation between the setpoint and actual motor speed.

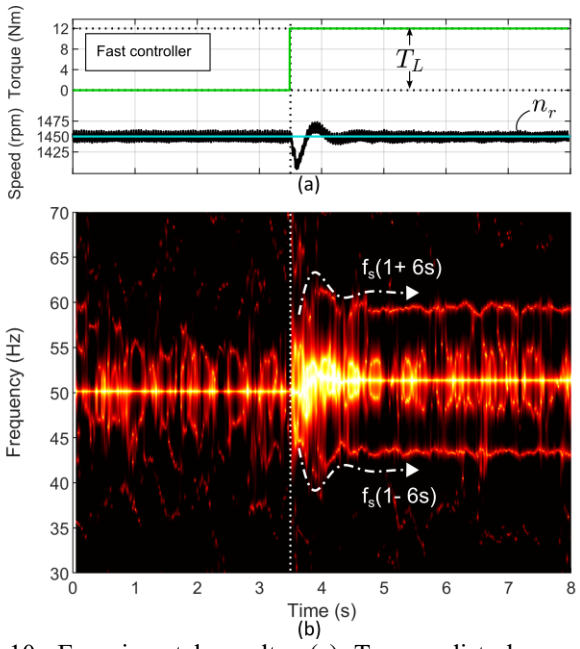

Fig. 10. Experimental results: (a) Torque disturbance and motor speed reaction; (b) T-f decomposition of the stator current, using the STMN, for the faulty motor under the fast PID controller and sudden torque disturbance.

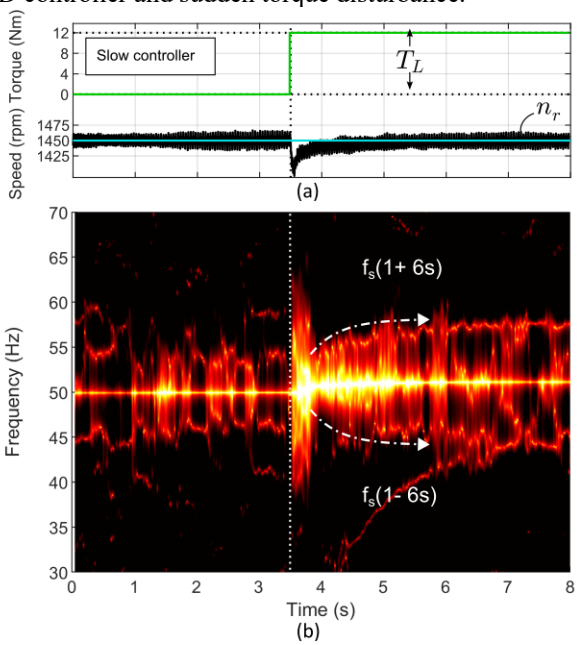

Fig. 11. Experimental results: (a) Torque disturbance and motor speed reaction, (b) T-f decomposition of the stator current, using the STMN, for the faulty motor under the slow PID controller and sudden torque disturbance.

Figures 10.b and 11.b show the *t-f* decomposition (computed with the STMN) of the stator current for the two PID cases. The load torque disturbance begins at 3.5 seconds. Before this, the motor operated at a very low load, the frequency of the fundamental component was very close to 50 Hz, and the fault harmonic components (Eq. 7 with *k=3*) could not be observed because the spectral distance between them and the dominant component is minimal, and there is spectral leakage around it. However, after the load disturbance

happens, the evolution of the fault-related harmonic components (Eq. 7 with $k = 3$) presents a different trajectory in the t-f plane depending on the PID controller type. In the case of the underdamped fast controller, these harmonics (Fig. 10.b) and the speed (Fig. 10.a) exhibit an oscillating course. In the other case, the response of the overdamped slow controller is very different because the trajectories of the fault-related harmonics show no signs of fluctuation (Fig. 11.b), and the speed settling time is more extended (Fig. 11.a), which also translates into a longer transient. In both cases, the inverter output main frequency increases (approximately 2 Hz) to compensate for the speed reduction caused by the sudden increment in the load torque. At the same time, this increase in frequency and current allows precise observation of the fault components $(1 \pm 6s)f_s$ because the spectral distance $6sf_s$ increases. In addition to the trajectories mentioned above, in Figure 11.b, there is a spectral component that is not associated with rotor defects and increases from 30 Hz to 45 Hz. This component can reach the fault-related harmonic and may cause a false positive or false negative error in fault diagnosis. These results underline the importance of time-frequency domain analysis. It is important to note that the control system significantly reduces speed variations under load changes and external disturbances. However, the inverter's corrective action generates new harmonic components that may interfere with the fault indicators commonly evaluated in the diagnostic algorithms currently in use.

VI. Conclusions

A study has been performed on the impact of PID control of an induction motor on the detection of BRB. This fault cannot be detected by classical analysis of the stator current when the control loop with speed as the reference signal is used. In addition, two types of PID controllers have been considered for the first time: overdamped and underdamped. In both cases, it has been observed that the noise level in the spectrum increases and that spectral leakage occurs around the main harmonic, which prevents the detection of the fault-related harmonics. The drive's response to the two types of control has been studied by subjecting it to speed step response and load torque perturbations. It is concluded that fault detection requires high-resolution time-frequency analysis. Two techniques have been proposed, the Dragon Transform and the STMN. The former allows visualisation of the third band of fault harmonics. Still, it is more sensitive to noise and frequency variations introduced by the controller in the underdamped case. In addition, it requires measuring the speed signal, which is not necessary for the STMN. This technique also has high-resolution and is immune to noise, but the fault visualisation is not as accurate. The fault is best detected in the *t-f* decompositions for the overdamped case. This study would have to be extended to inverters from other manufacturers and other types of faults. Consideration should also be given to how encoder quality affects control actions and fault detection. This study therefore demonstrates that BRB detection in controlled motors is an open issue. The result of this study is a method that allows to detect BRB fault when the motor is operating in closed-loop speed control. This result represents a novelty with respect to the literature, since it presents the following advantages: it is based on the analysis of a single stator current (normally measured in all the electrical drives, without adding any other sensor) and it is valid for different types of closed-loop control schemes.

Acknowledgment

The authors of this work would like to thank to Danfoss for donating the inverters used in this research. They also thank MathWorks Inc. for the encoder signal capture scripts.

References

[1] L. Frosini, “Novel diagnostic techniques for rotating electrical machines—A review,” *Energies*, vol. 13, no. 19, Art. no. 5066, 2020.

[2] S. B. Lee et al., “Condition monitoring of industrial electric machines: state of the art and future challenges,” *IEEE Ind. Electron. Mag.*, vol. 14, no. 4, pp. 158-167, Dec. 2020.

[3] J. Bonet-Jara, D. Morinigo-Sotelo, O. Duque-Perez, L. Serrano-Iribarnegaray, and J. Pons-Llinares, “End-ring wear in deep-well submersible motor pumps,” *IEEE Trans. Ind. Appl.*, vol. 58, no. 4, pp. 4522-4531, July-Aug. 2022.

[4] S. Halder, S. Bhat, D. Zychma, and P. Sowa, “Broken rotor bar fault diagnosis techniques based on motor current signature analysis for induction motor—A review,” *Energies*, vol. 15, Art. no. 8569, 2022.

[5] F. Filippetti, A. Bellini, and G.-A. Capolino, “Condition monitoring and diagnosis of rotor faults in induction machines: State of art and future perspectives,” in *Proc. WEMDCD*, Paris, France, 2013, pp. 196-209.

[6] A. Bellini, F. Filippetti, G. Franceschini, and C. Tassoni, “Closed-loop control impact on the diagnosis of induction motors faults,” *IEEE Trans. Ind. Appl.*, vol. 36, no. 5, pp. 1318-1329, Sept.-Oct. 2000.

[7] C. Kral, R. Wieser, F. Pirker, and M. Schagginger, “Sequences of field-oriented control for the detection of faulty rotor bars in induction machines—The Vienna monitoring method,” *IEEE Trans. Ind. Electron.*, vol. 47, no. 5, pp. 1042–1050, Oct. 2000.

[8] C. Kral, F. Pirker, and G. Pascoli, “Model-based detection of rotor faults without rotor position sensor—The sensorless Vienna monitoring method,” *IEEE Trans. Ind. Appl.*, vol. 41, no. 3, pp. 784–789, May/Jun. 2005.

[9] S. M. A. Cruz and A. J. M. Cardoso, “Diagnosis of rotor faults in direct and indirect FOC induction motor drives,” in *Proc. EPE*, Aalborg, Denmark, 2007, pp. 1–10.

[10] S. M. A. Cruz, A. Stefani, F. Filippetti, and A. J. M. Cardoso, “A new model-based technique for the diagnosis of rotor faults in RFOC induction motor drives,” *IEEE Trans. Ind. Electron.*, vol. 55, no. 12, pp. 4218-4228, Dec. 2008.

[11] Y. Gritli, A. O. Di Tommaso, R. Miceli, F. Filippetti, and C. Rossi, “Closed-loop bandwidth impact on MVSA for rotor broken bar diagnosis in IRFOC double squirrel cage induction motor drives,” in *Proc. ICCEP*, Alghero, Italy, 2013, pp. 529-534.

[12] S. S. Refaat, H. Abu-Rub, M. S. Saad and A. Iqbal, “Open and closed-loop motor control system with incipient broken rotor bar fault detection using current signature,” in *Proc. IECON*, Dallas, TX, USA, 2014, pp. 774–780.

[13] Z. Hou, J. Huang, H. Liu, T. Wang, and L. Zhao, “Quantitative broken rotor bar fault detection for closed-loop controlled induction motors,” *IET Electr. Power Appl.*, 2016, vol. 10, no. 5, pp. 403–410.

[14] Z. Hou, J. Huang, H. Liu, M. Ye, Z. Liu, and J. Yang, “Diagnosis of broken rotor bar fault in open- and closed-loop controlled wye-connected induction motors using zero-sequence voltage,” *IET Electr. Power Appl.*, 2017, vol. 11, no. 7, pp. 1214–1223.

[15] B. Asad, T. Vaimann, A. Belahcen, and A. Kallaste, “Broken rotor bar fault diagnostic of inverter fed induction motor using FFT, Hilbert and Park’s vector approach,” in *Proc. ICEM*, Alexandroupoli, Greece, 2018, pp. 2352-2358.

[16] H. Khelfi and S. Hamdani, “Mono-dimensional demodulation techniques for diagnosing broken rotor bars faults within inverter-fed induction machine at low load operation condition,” in *Proc. SDEMPED*, Dallas, TX, USA, 2021, pp. 512-517.

[17] L. Ralikalakala and P. Barendse, “Impact of inverter switching harmonics in detecting changes in impedance due to broken rotor bars,” in *Proc. ECCE*, Detroit, MI, USA, 2022, pp. 1-6.

[18] P. Wang, K. Wang, and L. Chen, “Broken rotor bars detection in inverter-fed induction motors under continuous switching of different speed modes,” *IEEE Trans. Ind. Electron.*, vol. 71, no. 1, pp. 975-984, Jan. 2024.

[19] V. Gurusamy, K. H. Baruti, M. Zafarani, W. Lee, and B. Akin, “Effect of magnets asymmetry on stray magnetic flux based bearing damage detection in PMSM,” *IEEE Access*, vol. 9, pp. 68849-68860, 2021.

[20] S. Huang, A. Aggarwal, E. G. Strangas, K. Li, F. Niu, and X. Huang, “Robust stator winding fault detection in PMSMs with respect to current controller bandwidth,” *IEEE Trans. Power Electron.*, vol. 36, no. 5, pp. 5032-5042, May 2021.

[21] F. Niu et al., “Robust inter-turn short-circuit fault detection in PMSGs With respect to the bandwidths of current and voltage controllers,” *IEEE Trans. Power Electron.*, vol. 38, no. 8, pp. 10269-10279, Aug. 2023.

[22] L. Mantione, V. Fernandez-Cavero, D. Morinigo-Sotelo and L. Frosini, “A Time-Frequency Analysis for Broken Rotor Bar Detection in Closed Loop Inverter Fed Induction Motor at Imposed Speed,” in *Proc. SDEMPED*, Chania, Greece, 2023, pp. 450–456.

[23] B. Yazici and G. B. Kliman, “An adaptive statistical time-frequency method for detection of broken bars and bearing faults in motors using stator current,” *IEEE Trans. Ind. Appl.*, vol. 35, no. 2, pp. 442-452, March-April 1999.

[24] V. Fernandez-Cavero, J. Pons-Llinares, O. Duque-Perez, and D. Morinigo-Sotelo, “Detection and quantification of bar breakage harmonics evolutions in inverter-fed motors through the dragon transform,” *ISA Trans.*, vol. 109, pp. 352–367, 2021.

[25] T.A. Garcia-Calva, D. Morinigo-Sotelo, O. Duque-Perez, A. Garcia-Perez, R.d.J Romero-Troncoso, “Time-Frequency Analysis Based on Minimum-Norm Spectral Estimation to Detect Induction Motor Faults,” *Energies*, vol. 13, Art. no. 4102, 2020.

[26] K. H. Nam, “AC Motor Control and Electrical Vehicle Applications,” *1st* ed. Boca Raton, Florida, U. S.: CRC Press, 2010.

[27] N. J. Antony, D. Mishra and S. Parveen, "Sensorless Field Oriented Control of AC Induction Motor Using PI, PD & PID Controllers," in *Proc.* IEEE (NKCon), Vijaypur, India, 2022, pp. 1-5.

[28] D. Rivera, M. Morari and S. Skogestad, "Internal model control: PID controller design", Industrial & Engineering Chemistry Process Design and Development, vol. 25, pp. 252-265, 1986.

[29] G. De Boni, V. Fernandez-Cavero, L. Frosini, O. Duque-Perez and D. Morinigo-Sotelo, "Fault Harmonics Current Detection in Closed-loop Controlled Induction Motors," in *Proc. IEEE SDEMPED*, Chania, Greece, 2023, pp. 443-449.

[30] J. Pons-Llinares, J. Antonino-Daviu, J. Roger-Folch, D. Moríñigo-Sotelo, and O. Duque-Pérez, “Mixed eccentricity diagnosis in inverter-fed induction motors via the adaptive slope transform of transient stator currents,” *Mech. Syst. Signal Process*, vol. 48, pp. 423–435, 2014.

[31] T. A. Garcia-Calva, K. N. Gyftakis, G. A. Skarmoutsos, M. Mueller, D. Morinigo-Sotelo and R. d. J. Romero-Troncoso, “Advanced Signal Processing Techniques for Demagnetization Detection in PM Generators at Variable Speed,” *IEEE Trans. Ind. Appl.*, vol. 60, no. 1, pp. 174-183, Jan.-Feb. 2024,

[32] F. Muzio, L. Mantione, T. Garcia-Calva, L. Frosini, and D. Moriñigo-Sotelo, "Detection of broken bars in induction motors operating with closed-loop speed control," Machines, vol. 12, Art. no. 662, 2024.

[33] Sul, Seung-Ki. *Control of Electric Machine Drive Systems*. Hoboken (New Jersey): Wiley-IEEE Press, 2011

[34] “How Does Closed Loop Control Work in a VFD?,” *KEB Automation KG*, Feb. 15, 2019. https://www.kebamerica.com/blog/how-does-closed-loop-control-work-in-a-vfd/

[35] M. A. Fnaiech et al., "A Measurement-Based Approach for Speed Control of Induction Machines," IEEE J. Emerg. Sel. Top. Power Electron., vol. 2, no. 2, pp. 308-318, June 2014.

[36] Yu, H. Shen, H. Wang and X. Wu, "Speed Estimation of Multiphase Induction Motor Using Rotor Slot Harmonics With Limited SNR and Dynamic Load Conditions," *IEEE Trans. Ind. Electron.*, vol. 70, no. 7, pp. 6618-6631, July 2023.

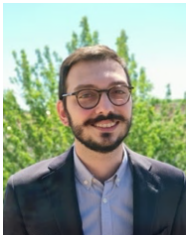

Lorenzo Mantione (Student Member, IEEE) received his BSc (2017) and MSc (2020) in Electrical Engineering at University of Pavia, where he is a PhD student in Electrical Engineering. His research interests include condition monitoring and fault diagnostics of electric motors, and design of electrical machines.

Tomas Garcia-Calva (Member, IEEE), received the M. E. and the Ph.D. degrees in Electrical Engineering from the University of Guanajuato, México, in 2016 and 2021, respectively. He was an intern with the Polytechnic University of Valencia, Spain in 2016, and with the University of Valladolid, Spain in 2019. He is currently a Research Assistant with the University of Valladolid, Spain. His research interests include digital signal processing, data analysis, and condition monitoring of electric machines.

Vanesa Fernandez-Cavero, received her B.S. in industrial organization and electrical engineering from ICAI, Comillas Pontifical University, Madrid, in 2005, and her Ph.D. in electrical engineering from the University of Valladolid in 2018. She is a Professor at the University of Burgos. Her research focuses on monitoring induction machines and diagnosing faults in inverter-fed IM during transients.

Lucia Frosini (Member, IEEE), received the MSc (1994) and the PhD (2000) degrees in Electrical Engineering at University of Pavia, where she is associate professor of Diagnostics for electrical machines, Design and technology of electrical machines and Electrical drives. Her research interests include design, modelling, simulation and diagnostics of rotating electrical machines and transformers.

Daniel Morinigo-Sotelo (Member, IEEE), received the B.S. and Ph.D. degrees in electrical engineering from the University of Valladolid (UVA), Spain, in 1999 and 2006, respectively. He is currently with the Research Groups HSPDigital and Analysis and Diagnostics of Electrical Grids and Installations (ADIRE), which belongs to the ITAP Institute (UVA), and with the HSPdigital Research Group, México. His current research interests include fault detection and diagnostics of induction machines, power quality, and smart grids.